Satellites in the inviscid breakup of bubbles

J.M. Gordillo*

Departamento de Ingeniería Aeroespacial y Mecánica de Fluidos. Universidad de Sevilla. Avda. de los Descubrimientos s/n, 41092, Sevilla, SPAIN.

M.A. Fontelos†

Departamento de Matemáticas, Consejo Superior de Investigaciones Científicas, C/ Serrano 123, 28006 Madrid, Spain.

(Dated: February 12, 2007)

Abstract

In this letter, we stress the essential role played by gas inertia in the breakup of gas bubbles. Our results reveal that, whenever the gas to liquid density ratio $\Lambda = \rho_g/\rho_l$ is different from zero, tiny satellite bubbles may be formed as a result of the large gas velocities that are reached close to pinch-off. Moreover, we provide with a closed expression for the characteristic satellite diameter, which decreases when decreasing Λ and which shows order of magnitude agreement with the micron-sized satellite bubbles observed experimentally.

*jgordill@us.es

†marco.fontelos@uam.es

The breakup of an air bubble in water is one of the most common processes of daily life. The detailed analytical description of bubble formation and subsequent breakup started over a decade ago with two landmark papers by Longuet-Higgins et al [1] and Oguz and Prosperetti [2]. However, our understanding of such ubiquitous phenomenon is not yet fully satisfactory compared with the analogous problem of drop breakup in air [3]. One of the aspects that still deserves further study is the description of the time evolution of the region near the minimum radius at instants close to pinch-off [3], which will be useful, among other things, as an intermediate step to scale the high-speed Worthington jets formed when rain drops [4], or a solid object [5] impact on a free surface, a phenomenon also observed in the collapse of a cylindrical air cavity [6], or in the breakup of bubbles injected from an underwater nozzle within a liquid co-flow [7].

Previous studies regarding the breakup of inviscid liquid drops in air [8–10] found that the minimum radius decreased in time as $R_0 \propto (t_0 - t)^\alpha$, with t_0 the pinchoff time and $\alpha = 2/3$. The 2/3 exponent, which is universal and independent of initial conditions, arises as a consequence of the fact that the local dynamics is governed by a balance between surface tension and liquid inertia. The same exponent might be expected to describe the pinch-off of bubbles as well. However, Burton, Waldrep and Taborek [11] showed that the exponent describing the time evolution of the minimum radius for the (common) case of breakup of air bubbles in water, is very close to $\alpha = 1/2$ and also reported, for the first time, the formation of micron-sized satellites. Albeit the deviation from the $\alpha = 2/3$ exponent had been already predicted by [1, 2], a great interest arose as a consequence of further experimental evidence, which demonstrated that α varied between 0.59 and 0.55 [5, 12, 13], what was interpreted as a sign of non-universality.

In what follows it will be shown that, as the singularity is approached, gas inertia comes into play no matter how small the inner to outer density ratio is, provoking the first pinch of the bubble to take place at $z \neq 0$ in spite of the initial mirror symmetry of the bubble and boundary conditions around $z = 0$. The main consequences of this fact are: i) the experimental observation of *tiny* satellites in the inviscid breakup of bubbles [11–13], which lacked of explanation, can be now understood and attributed to the finiteness of gas density, ii) the very final stages of the time evolution of α are not predicted neither by the theory presented in [14] nor in that of [15], iii) the experimentally measured values of α correspond to an *intermediate* asymptotic limit before the satellite begins to form.

In the numerical simulations reported below, the bubble is placed symmetrically within a

straining flow, as done in [16, 17]. The type of outer flow imposed leads to bubble breakup for a sufficiently large value of the Weber number (fixed to 48) but does not affect to the local dynamics near pinch-off. Figure 1, where axial and radial distances are made dimensionless using the initial (spherical) bubble radius, shows the time evolution of the bubble surface for $\Lambda = 0.005$ (four times the air to water density ratio). The striking result of this figure is that an *elongated* satellite bubble (in agreement with experimental observations by [13]) begins to form at exceedingly small radial and axial length scales. Note that, as explained below, the critical radius, r_c, defined here as the one at which the (time dependent) curvature at $z = 0$ reaches a maximum, decreases dramatically as the density ratio is lowered. This is the reason why the generation of satellites was previously reported in the case of drop breakup [9, 10, 16] but not in the numerical and analytical studies of bubble breakup.

In order to explain the mechanism leading to the *symmetric* type of breakup (in the sense given in [17]) to form satellites, it proves convenient to plot both the liquid normal velocities and the tangential gas velocities at the bubble free surface (see Fig. 2). As depicted from figure 2a, the absolute value of the normal velocities present a maximum at $z = 0$ for a value of $R_0 = 0.0196$ (R_0 is defined here as the radius at $z = 0$). Nevertheless, as the collapse process advances, the maximum of the absolute value of the normal velocity is displaced from $z = 0$ (see the curve for $R_0 = 0.00425$). The reason for this displacement can be found in Fig. 2b, where it is shown that gas velocities increase with the axial distance z in an approximate linear way until a maximum is reached. Indeed, in order to accelerate the gas longitudinally, there must exist a maximum in the pressure at $z = 0$, being the gas pressure difference given by $p_g(0) - p_g(\ell) \sim \rho_g\, v_g^2(\ell)$. In the previous expression, the subscript g denotes 'gas' and $v_g(\ell)$ the maximum of the longitudinal gas velocity occurring at a characteristic axial length scale ℓ. Note that continuity demands that $2\pi R_0 \ell dR_0/dt \simeq \pi R_0^2 v_g(\ell)$ and, consequently, $p_g(0) - p_g(\ell) \sim \rho_g(\ell/R_0^2)^2\,(dR_0^2/dt)^2$. Due to the fact that the liquid convective acceleration can be estimated as $\sim \rho_l(1/R_0^2)\,(dR_0^2/dt)^2$, with the subscript l indicating 'liquid', the ratio $\rho_l\,(1/R_0^2)\,(dR_0^2/dt)^2/[p_g(0) - p_g(\ell)] \sim \rho_l/\rho_g(R_0/\ell)^2$. The fact that the local bubble shape becomes more and more slender as the singularity is approached [14, 15, 17] implies that $(R_0/\ell)^2$ decreases in time and, therefore, $\rho_l/\rho_g(R_0/\ell)^2$ becomes of order unity at some instant previous to pinch-off. Moreover, as observed by comparing the last two profiles in Fig. 2a, there exists a range of values of R_0 for which the gas overpressure at $z = 0$ is able to decelerate the inward radial motion of the liquid, whereas the lower pressure at $z \sim \ell$ is able to accelerate inwards the liquid through the suction mechanism described in [17]. Note

also that the deceleration at $z = 0$ can be quite strong as observed in Fig. 2 and this might lead to the development of a Rayleigh-Taylor instability. This qualitative description is supported by the result in Fig. 2c, where the ratio $\rho_l\, v_n^2/\rho_g\, v_g^2$, with v_n the maximum normal liquid velocity and v_g the maximum axial gas velocity, decreases when decreasing R_0. Moreover, it is also observed in this figure that the typical radius for which $\rho_l\, v_n^2/\rho_g\, v_g^2 \sim O(1)$ decreases dramatically as Λ decreases and, therefore, the smaller the density ratio is, the smaller is the length scale for which the satellite bubble begins to form.

The fact that gas inertia must come into play at some instant previous to pinch off is also reflected in the time evolution of the instantaneous exponent α [15], as depicted in Fig. 3. Here we compare the numerically calculated value of α with $\alpha_1 = 1/2\,(1 + 1/(4 \ln R_0))^{-1}$ [5, 14, 17] which, for $\tau \gg 1$, being $\tau = -\ln(t_0 - t)$, is such that $\alpha_1 \to 1/2 + 1/(4\,\tau)$ and $\alpha_2 = 1/2 + 1/(4\sqrt{\tau})$ [15]. Note from this figure that the numerical solution lies between both asymptotic expressions but is quite closer to that given by [15] during a finite and intermediate range of times. Nevertheless, α drops to zero for sufficiently small values of R_0 as a consequence of the increasingly larger pressures at $z = 0$ needed to accelerate the gas longitudinally.

It is now our purpose to develop a simple model which, retaining the dominant physical mechanisms described above, permits us to both reproduce the time evolution of the exponent α in Fig. 3 and to scale the size of the satellite bubbles obtained as a function of Λ. For this purpose, and as suggested by the good agreement depicted in Fig. 3, we will simply complement equations (4)-(6) in [15] by adding the effect of gas inertia.

Under the slenderness approximation, gas velocity can be calculated using continuity which demands, at leading order in z,

$$v_g(z) = -\frac{1}{R_0^2}\,\frac{d\,R_0^2}{d\,t}\,z\,. \tag{1}$$

On the other hand, the integration between $z = \ell$ and a generic axial position z of the incompressible, slender and inviscid momentum equation projected in the longitudinal direction yields, at leading order in z,

$$p_g(0) = p(\ell) + \rho_g \left[\frac{2}{R_0^4}\left(\frac{d\,R_0^2}{d\,t}\right)^2 - \frac{1}{R_0^2}\,\frac{d^2\,R_0^2}{d\,t^2}\right]\frac{\ell^2}{2}, \tag{2}$$

and

$$p_g(z) = p(0) - \rho_g \left[\frac{2}{R_0^4}\left(\frac{d\,R_0^2}{d\,t}\right)^2 - \frac{1}{R_0^2}\,\frac{d^2\,R_0^2}{d\,t^2}\right]\frac{z^2}{2}\,. \tag{3}$$

Taking into account that $\ell = \sqrt{R_0\,R_c} = (R_0/d^2R/d\,z^2|_{z=0})^{1/2}$, with R_c the radius of curvature of the interface at $z = 0$ [5, 14, 15] and $d^2R(z)/d\,z^2|_{z=0} = 1/R_c$, the following coupled set of

equations for α and the aspect ratio $a'' \equiv d^2\, R_0^2/d\, z^2|_{z=0} = 2\, R_0/R_c$ is obtained, [15]:

$$\left(\alpha_\tau + \alpha - 2\alpha^2\right)\, \ln\left(\Gamma_1/a''\right) = -\alpha^2 - 4\Lambda/a''\left(\alpha_\tau + \alpha + 2\alpha^2\right) \tag{4}$$

$$\left(\delta_\tau + \delta - 2\delta^2\right)\, \ln\left(\Gamma_2/a''\right) = -3\alpha^2 + 2\,\alpha - 2\alpha\delta + 2\alpha_\tau + 4\Lambda/a''\left(\alpha_\tau + \alpha + 2\alpha^2\right) \tag{5}$$

$$\ln\left(a''\right)_\tau = -2\delta\,, \tag{6}$$

with Γ_1 and Γ_2 order unity constants and the subscript τ denoting τ derivatives. In addition, note that δ is simply an intermediate variable that couples α with R_c/R_0. It is simple to verify that the system (4)-(6) has two time independent solution located at $[\alpha, \delta, \ln\left(a''\right)] = ((2 + 2\Lambda e^2)/(3 - 8\Lambda e^2), 0, -2)$, and $[\alpha, \delta, \ln\left(a''\right)] = (0, 0, C_0)$, with C_0 a constant. Nevertheless, the former solution is unstable whereas the latter is stable but represents no evolution. Therefore, as suggested in Fig. 3, the true solution for $\Lambda \ll 1$ is the one such that, in the limits $\Lambda = 0$, $\tau \gg 1$ behaves as [15]

$$\alpha \sim 1/2 + 1/(4\sqrt{\tau})\ ,\ \delta \sim 1/(4\sqrt{\tau})\ ,\ \ln\left(a''\right) \sim -\sqrt{\tau}\,. \tag{7}$$

As depicted in Fig. 4, the integration of the system (4)-(6), with the correct behaviors given in (7) is able to accurately reproduce the time evolution of α and, therefore, it contains all the essential ingredients of the inviscid bubble pinch-off in the incompressible approach. Moreover, in order to estimate the typical dimensionless diameter of the satellite bubbles formed, d_b, it proves convenient to define $\Phi = a''/\Gamma_1$ which, in the limits $\Lambda = 0$, $\tau \gg 1$ behaves as $e^{-\sqrt{\tau}}$. Note that, once the correct behaviors of Φ and α for large τ are introduced into Eq. (4), the characteristic value τ_c for which the ratio of liquid to gas momentum becomes of order unity ($\rho_l\, v_n^2/\rho_g\, v_g^2 \sim O(1)$) can be calculated by balancing the two terms on the right of Eq. (4) as

$$\frac{4\Lambda}{\Gamma_1\,\Phi} \sim \frac{1}{4} \rightarrow \tau_c = \left[\ln\left(\frac{16\Lambda}{\Gamma^*}\right)\right]^2\,, \tag{8}$$

where Γ^* absorbs the proportionality factor in (8) (~ 0.5). The estimate of the critical radius as a function of Λ can be calculated as

$$r_c = A\, e^{-\tau_c \alpha(\tau_c)} = A\, e^{-\frac{1}{2}\tau_c - \frac{\sqrt{\tau_c}}{4} + O(\tau_c^{-\frac{1}{2}})} = A\left(\frac{16\Lambda}{\Gamma^*}\right)^{\frac{1}{4}}\ e^{-\frac{1}{2}\left[\ln\left(\frac{16}{\Gamma^*}\Lambda\right)\right]^2}\,, \tag{9}$$

being A a constant that depends on initial conditions.

The inset in Fig. 4 shows that the transition radii obtained numerically for different values of the Weber number and those predicted by Eq. (9) are in excellent agreement for $\Gamma^* = 2$ if A is fixed to 1; also observe the slight dependence on initial conditions (different initial Weber

numbers). Note that other initial or boundary conditions may provide different values of Γ^* and A. Finally, bubble diameter is given by, $d_b \sim (6\,\ell_c/r_c)^{1/3}\,r_c \propto r_c$, with the air ligament aspect ratio obtained from the numerical simulations ranging from $\ell_c/r_c \sim 10-20$. Note that, from the data shown in the inset of Fig. 4, the size of the satellite bubbles ranges, depending on the value of $\Lambda \in (10^{-3}, 10^{-2})$, between $\sim 10^{-5}$ to $\sim 10^{-3}$ times the initial bubble radius, and this explains the tiny satellite bubbles ($\sim O(1\mu\,m)$) observed experimentally [11–13].

Other factors, not taken into account in the deduction of Eq. (9), may influence quantitatively the size of the resulting satellites. These are: i) Compressibility effects [18], ii) Satellite breakup [19], iii) The slow (logarithmic) convergence [14] to the asymptotic limit favors the formation of satellites at a length scale which could be larger than the one at which the asymptotic limit in [15] is reached. In that case, use of Eq. (9) is not justified [20].

The authors are grateful to A. Sevilla, J. Rodríguez-Rodríguez and C. Martínez-Bazán for their careful reading of the manuscript and suggestions. We also thank Prof. S.T. Thoroddsen for very useful comments and Prof. J. Eggers and Dr. J. Snoeijer for discussions. This research has been supported by the Spanish Ministry of Education under project # DPI2005-08654-C04-02.

[1] M. S. Longuet-Higgins, B. R. Kerman, and K. Lunde, J. Fluid Mech. **230**, 365 (1991).

[2] H. Oguz and A. Prosperetti, J. Fluid Mech. **257**, 111 (1993).

[3] J. Eggers, Rev. Mod. Phys. **69**, 865 (1997).

[4] A. Worthington, Longman and Green, London (1908).

[5] R. Bergmann and et al, Phys. Rev. Lett. **96**, 154505 (2006).

[6] D. Bartolo, C. Josserand, and D. Bonn, Phys. Rev. Lett. **96**, 124501 (2006).

[7] J. Gordillo and et al., Submitted to Phys. Fluids (2006).

[8] Y. Chen and P. Steen, J. Fluid Mech. **341**, 245 (1997).

[9] R. F. Day, E. J. Hinch, and J. R. Lister, Physical Review Letters **80**, 704 (1998).

[10] D. Leppinen and J. R. Lister, Phys. Fluids **15**, 568 (2003).

[11] J. Burton, R. Waldrep, and P. Taborek, Phys. Rev. Lett. **94**, 184502 (2005).

[12] N. Keim, P. Moller, W. Zhang, and S. Nagel, Phys. Rev. Lett. **97**, 144503 (2006).

[13] S. Thoroddsen, T. Etoh, and K. Takehara, Submitted to Phys. Fluids (2006).

[14] J. Gordillo and M. Pérez-Saborid, J. Fluid Mech. **562**, 303 (2006).

[15] J. Eggers and et al, http://arxiv.org/abs/physics/0610139 (2006).

[16] J. Rodríguez-Rodríguez, J. M. Gordillo, and C. Martínez-Bazán, J. Fluid Mech. **548**, 69 (2006).

[17] J. Gordillo and et al, Phys. Rev. Lett. **95**, 194501 (2005).

[18] Relative density variations can be estimated as $\Delta\,\rho_g/\rho_g \sim\ M_g^2$, with M_g the gas Mach number. In order to estimate M_g note that satellites are formed if $\rho_g\,\hat{v}_g^2 \simeq K\rho_l\,\hat{v}_l^2\,, \hat{v}_g \simeq 0.7(\rho_l/\rho_g)^{1/2}\,\hat{v}_l$ ($K = 0.5$, and *hats* indicating dimensional quantities) and liquid velocity close to pinch-off, $\hat{v}_l \simeq 5\,m\,s^{-1}$ under the experimental conditions of [13]. Therefore, our incompressible assumption is realistic under these conditions since, in the case of air, $\Delta\,\rho_g/\rho_g \sim 0.15$ at room temperature. Nevertheless, the strong dependence of r_c on Λ in (9) suggests the inclusion of compressibility effects (currently under way) since r_c will be larger due to the larger gas density.

[19] As pointed out by A. Sevilla (personal communication), the satellite bubble may also split in two as a consequence of the fact that the Weber number characterizing the local axisymmetric straining flow surrounding the satellite (see [14] for details) is above the critical one [16]. In addition, the breakup of subsatellites could form sub-subsatellites.

[20] This restriction applies, specially, to the larger values of Λ (larger r_c).

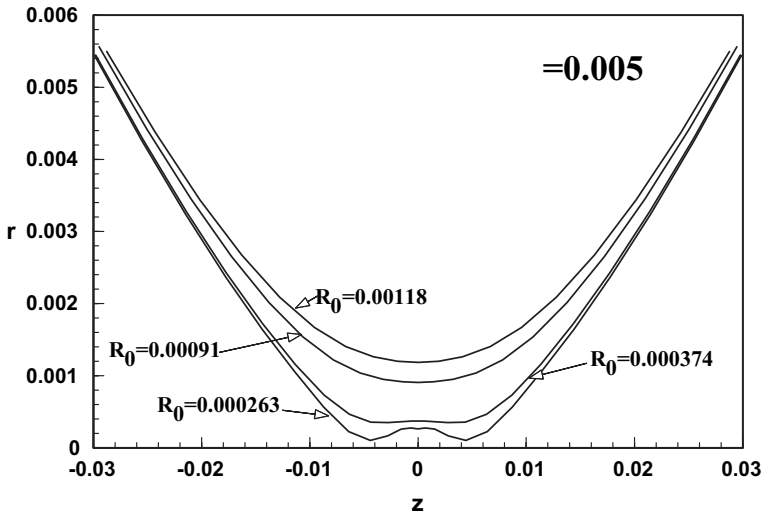

FIG. 1: Evolution of bubble shapes for times close to pinch-off showing that an elongated satellite bubble is formed.

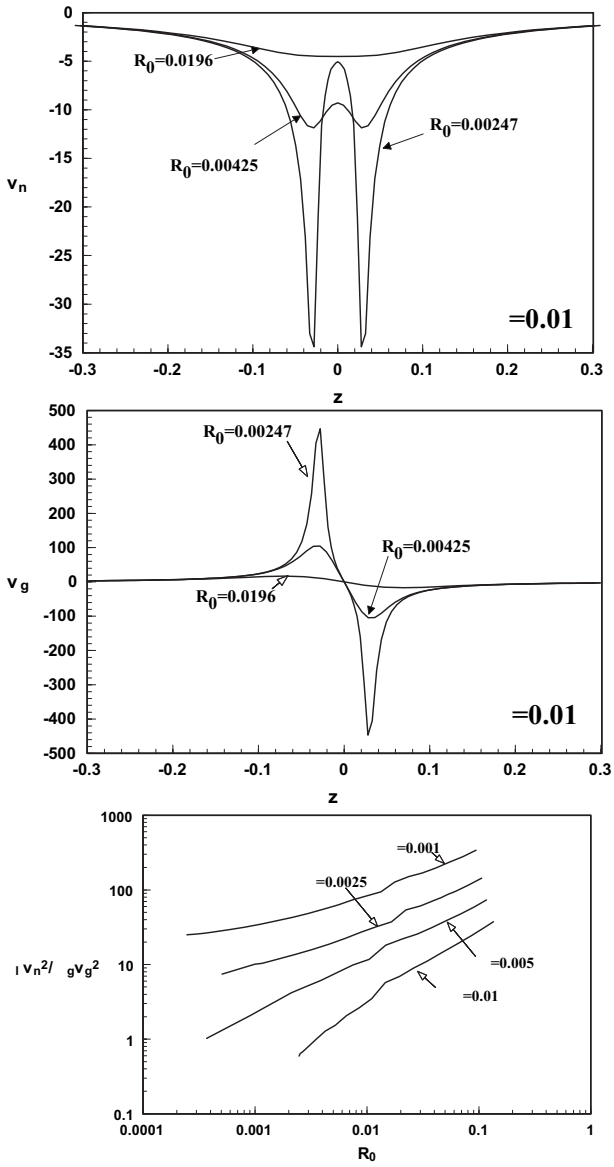

FIG. 2: a) Axial variation of normal velocities at the interface for three different values of R_0. b) Axial distribution of tangential gas velocities for three different values of R_0. c) Ratio of the maximum value of the liquid convective inertia ($\rho_l\, v_n^2$) to the maximum value of gas convective inertia ($\rho_g\, v_g^2$)

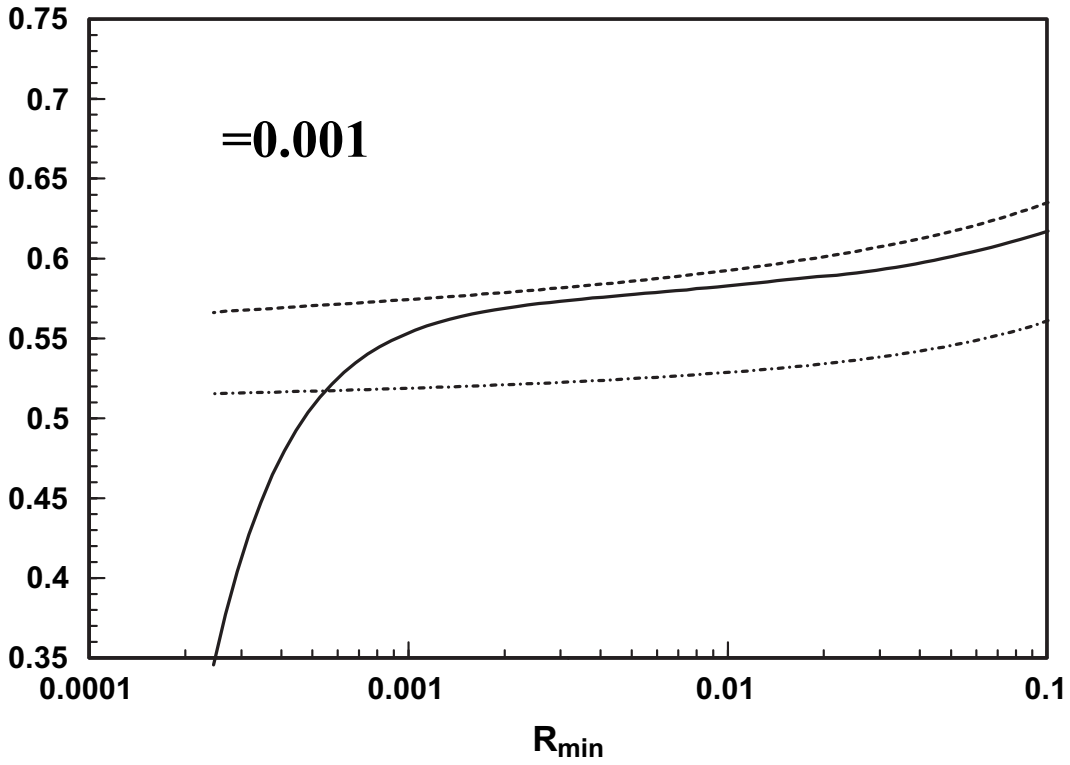

FIG. 3: Time evolution of the numerically calculated instantaneous exponent α [15] (continuous line) and the asymptotic predictions given in [14] (dotted-dashed line) and [15] (dashed line) shows that α drops to zero for sufficiently small values of R_0 as a consequence of the increasingly larger pressures at $z = 0$ needed to accelerate the gas longitudinally.

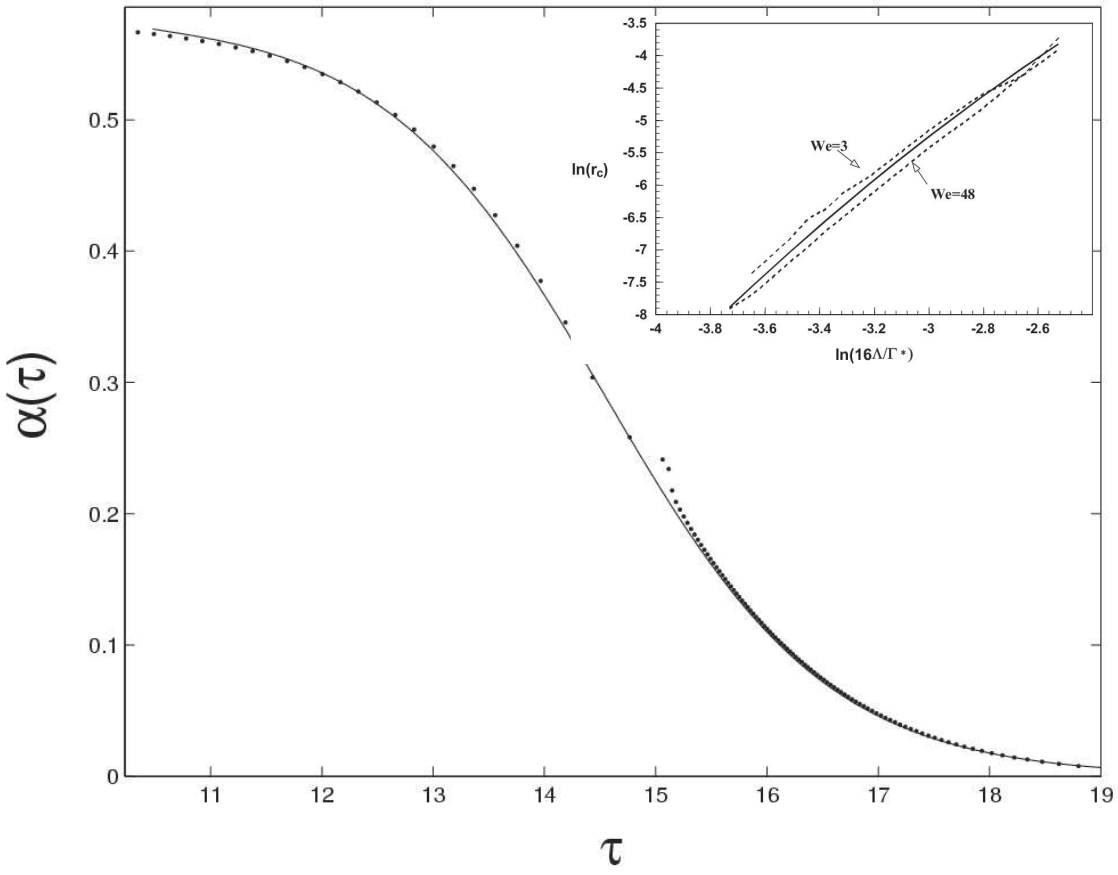

FIG. 4: Comparison of $\alpha(\tau)$ calculated from the full numerical simulations (dots) and by solving the system (4)-(6) (case of $\Lambda = 0.001$ in Fig. 3). Note that, for $\tau > 15$, the numerical results are affected by an instability triggered by the large gas velocities. Inset: numerical (dashed lines) and theoretical (continuous line) values of r_c vs Λ for two values of the initial Weber number. Note that the critical radius, r_c, is obtained from the numerical simulations as the one at which the time dependent axial curvature reaches a maximum. The continuous line represents Eq. (9), with $A = 1$ and $\Gamma^* = 2$. The smaller value of Λ in this figure is $\Lambda = 3 \times 10^{-3}$.